

# Cooperative Tri-Point Model-Based Ground-to-Air Coverage Extension in Beyond 5G Networks

Ziwei Cai, Min Sheng, Junyu Liu, Chenxi Zhao, and Jiandong Li

State Key Laboratory of Integrated Service Networks, Xidian University, Xi'an, Shaanxi, 710071, China

## Abstract

The utilization of existing terrestrial infrastructures to provide coverage for aerial users is a potentially low-cost solution. However, the already deployed terrestrial base stations (TBSs) result in weak ground-to-air (G2A) coverage due to the down-tilted antennas. Furthermore, achieving optimal coverage across the entire airspace through antenna adjustment is challenging due to the complex signal coverage requirements in three-dimensional space, especially in the vertical direction. In this paper, we propose a cooperative tri-point (CoTP) model-based method that utilizes cooperative beams to enhance the G2A coverage extension. To utilize existing TBSs for establishing effective cooperation, we prove that the cooperation among three TBSs can ensure G2A coverage with a minimum coverage overlap, and design the CoTP model to analyze the G2A coverage extension. Using the model, a cooperative coverage structure based on Delaunay triangulation is designed to divide triangular prism-shaped subspaces and corresponding TBS cooperation sets. To enable TBSs in the cooperation set to cover different height subspaces while maintaining ground coverage, we design a cooperative beam generation algorithm to maximize the coverage in the triangular prism-shaped airspace. The simulation results and field trials demonstrate that the proposed method can efficiently enhance the G2A coverage extension while guaranteeing ground coverage.

## Index Terms

G2A coverage extension; CoTP model; cooperative beam;

## I. INTRODUCTION

With the popularity of aerial applications, including public safety patrol, cargo transport, and traffic monitoring, aerial user equipments (AUEs) have been soaring globally over recent years [1], [2]. Enabling AUEs-centric applications requires ubiquitous wireless connectivity in beyond-5G (fifth generation) networks. The terrestrial cellular network is a natural candidate for serving AUEs [3], since it can take advantage of existing ground infrastructures and coverage technologies to provide radio access services at low cost. However, it is challenging to efficiently extend coverage from the ground to three-dimensional (3D) airspace by leveraging the current terrestrial infrastructure due to the down-tilted antennas of terrestrial base stations (TBSs) fail to meet the coverage demand in the vertical direction [4]. Although antennas can be tilted upward, it is still difficult to design the optimal beam to efficiently cover 3D airspace since it is a multi-objective optimization problem that involves maximizing coverage while minimizing overlap [5]. Therefore, we intend to provide answers to the following questions for ground-to-air (G2A) coverage extension: 1) how to design the cooperative coverage structure based on the deployed TBSs, and 2) how to optimize antenna beam parameters of cooperative TBSs to implement cooperative airspace coverage.

### A. Related Work and Motivation

The coverage enhancement methods of terrestrial cellular networks have been widely studied over the past decades [6]–[8]. These studies have focused on investigating methods to optimize ground coverage by adjusting antennas. However, they ignore the coverage demand in the vertical direction, which is an important feature of the G2A coverage extension [9]. Regarding the G2A coverage, the use of a down-tilted antenna may lead to coverage holes. This is attributed to the fact that the down-tilted antenna primarily serves the airspace above it through its side lobes [10], [11].

Considering the importance and distinctiveness of the G2A coverage, recent studies are exploring ways to enhance coverage for airspace. The first study attempting to provide a comprehensive analysis of the G2A coverage extension can be traced back to [12], which outlines a potential pathway for achieving airspace coverage. The authors of [13] have investigated the potential and challenges of G2A coverage extension, highlighting that advanced antenna technologies have the ability to enhance the coverage of airspace. In [14], the authors have offered a link-level coverage analysis of the cellular network that serves both AUEs and ground users. Meanwhile, the hand-off of AUEs and the coverage probability of AUEs have been analyzed in [15]. Although these studies provide the theoretical analysis of the link-level coverage ability of airspace based on stochastic geometry, they fail to provide a practical solution to enhance the G2A coverage extension.

With the advancement of 3D directional antenna technology, adjustable antenna parameters of TBS can be used to enhance the G2A coverage extension. The ability to improve the coverage performance by adjusting the tilt angle and beam-width of the antenna has been demonstrated in [5]. However, it fails to consider how to fulfill the coverage requirements across the entire airspace with different heights. For the deployed TBSs, the challenge in enhancing the G2A coverage stems from extending coverage into the airspace while ensuring ground coverage.

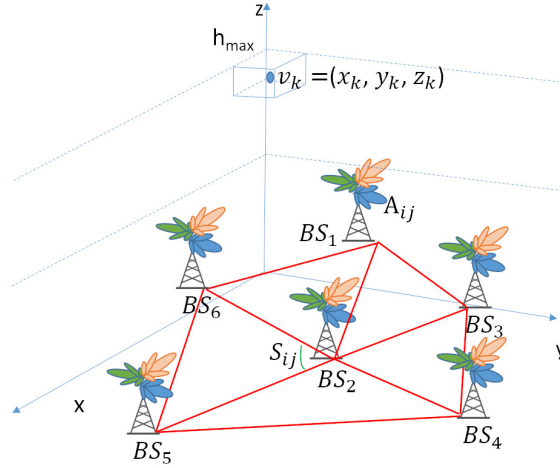


Fig. 1. Illustration of the cellular network for G2A coverage extension.

## B. Outcomes and Contributions

Motivated by the above discussions, in this work, we propose a G2A coverage extension method based on the cooperative tri-point (CoTP) model. The outcomes and contributions of this paper can be summarized as follows:

- We prove the property of achieving minimum overlap through the cooperation coverage among three TBSs. Subsequently, a CoTP model is proposed to analyze the G2A coverage extension in existing cellular networks. Based on this, a Delaunay triangulation (DT)-based cooperative coverage structure is designed to seamlessly divide a given airspace into multiple triangular prism (TP)-shaped airspaces and formulate corresponding TBS cooperation sets.
- We design two cooperative beam generation algorithms to maximize the coverage ratio of each TP-shaped airspace while controlling overlap ratio. Especially, the space-layered beam cooperative (SLBC) coverage algorithm is designed to efficiently cover the low, medium, and high-layered subspaces by tuning the discrete antenna pattern. Moreover, the adaptive beam cooperative (ABC) coverage algorithm is designed to further enhance 3D coverage and prevent power leakage by generating beams with continuously adjustable bandwidth.
- We conduct extensive simulations as well as field trials, which demonstrate that the proposed method can improve the coverage ratio of 3D airspace by 83% compared to a cellular network that uses down-tilted antenna parameters, while also guaranteeing ground coverage.

The following sections of this paper are organized as follows. In Section II, we present the system model and introduce performance metrics. In Section III, we propose the CoTP-based G2A coverage extension method. The simulations and field trials are presented in Section IV. Finally, conclusions are drawn in Section V.

## II. SYSTEM MODEL

### A. Network Model

We consider a cellular network for G2A coverage extension (see Fig. 1), which consists of TBSs (with the same transmit power) denoted by  $\Pi_{\text{BS}} = \{\text{BS}_i \mid i = 1, 2, \dots, I\}$  and sectors denoted by  $\Pi_{\text{S}} = \{S_{ij} \mid i = 1, 2, \dots, I, j = 1, 2, \dots, J\}$ , where  $S_{ij}$  denotes the  $j$ -th sector of  $i$ -th TBS. The sets of antennas of TBSs are denoted by  $\Pi_{\text{A}} = \{A_{ij} \mid i = 1, 2, \dots, I, j = 1, 2, \dots, J\}$ . Each sector  $S_{ij}$  is equipped with one 3D directional antenna  $A_{ij}$ . The horizontal half-power bandwidth (H-HPBW), vertical half-power bandwidth (V-HPBW), and tilt angle of each antenna are denoted by  $\epsilon = \{\Psi, \Phi, \Theta\}$ . The 3D Cartesian coordinate of  $\text{BS}_i$  is denoted as  $(x_{\text{BS}_i}, y_{\text{BS}_i}, z_{\text{BS}_i})$ . The directional antenna beams with different patterns can provide wireless coverage for the low-altitude 3D airspace  $\Omega$ . The maximal height of  $\Omega$  is denoted by  $h_{\text{max}}$ .

The 3D continuous airspace  $\Omega$  can be discretized by a regular cubic lattice [16], which is denoted by  $\mathbf{v}_k = (x_k, y_k, z_k)$ . Specifically, the coverage ratio of the center point of lattice represents that of the entire lattice. The number of lattices in the airspace  $\Omega$  is denoted by  $N_t$ . The tilt angle  $\Theta$  determines the direction of the directional beam, thereby affecting the received power of each lattice.

### B. Channel Model and Antenna Model

The G2A channel model of lattice  $\mathbf{v}_k = (x_k, y_k, z_k)$  is given by

$$PL(d_{2D}, h_t) = p_L PL_L + p_N PL_N, \quad (1)$$

where the two-dimensional distance between the TBS and lattice  $\mathbf{v}_k$  is given by  $d_{2D} = \sqrt{(x_{v_k} - x_{BS_i})^2 + (y_{v_k} - y_{BS_i})^2}$ , while the height difference between them is expressed as  $h_t = \sqrt{(z_{v_k} - z_{BS_i})^2}$ . Moreover,  $PL_L$  and  $PL_N$  denote the path loss in the line-of-sight (LOS) condition and the non-line-of-sight (NLOS) condition, respectively.  $p_L$  and  $p_N$  denote the LOS probability and the NLOS probability, respectively. The coefficients of the channel model are given by the 3GPP technical report TR36.777 [17].

The 3D directional antenna gain [18] is given by

$$G(\varphi, \phi) = \begin{cases} G_0/(\Psi \times \Phi), & -\Psi \leq \varphi \leq \Psi, -\Phi \leq \phi \leq \Phi, \\ S_0, & \text{otherwise,} \end{cases} \quad (2)$$

where  $\Psi \in (0, \pi)$ ,  $\Phi \in (0, \pi)$ ,  $G_0 = 2.2864$  and  $S_0 = 0.03$  [19].

### C. Performance Matrices and Problem Formulation

The received power of lattice  $\mathbf{v}_k = (x_k, y_k, z_k)$  is given by

$$P_{BS_i}(\mathbf{v}_k) = P_T + G_{BS_i}(\varphi_{\mathbf{v}_k}, \phi_{\mathbf{v}_k}) + PL_{BS_i}(\mathbf{v}_k), \quad (3)$$

where  $P_T$  and  $G_{BS_i}(\varphi_{\mathbf{v}_k}, \phi_{\mathbf{v}_k})$  are the transmit power and the antenna gain of  $BS_i$ , respectively, and  $PL_{BS_i}(\mathbf{v}_k)$  is the path loss of the G2A channel.

In this paper, we employ the good coverage ratio (GCR) and the coverage overlap ratio (COR) for evaluating the G2A coverage extension [20]. Let  $\xi$  denotes the GCR, we have

$$\xi = \frac{N_{\text{cov}}}{N_t}, \quad (4)$$

where  $N_{\text{cov}}$  denotes the number of lattices with received power that exceeds the received power threshold.  $N_{\text{cov}}$  is given by

$$N_{\text{cov}} = \sum_{k=1}^{N_t} C(\mathbf{v}_k), \quad (5)$$

where  $C(\mathbf{v}_k)$  denotes whether the lattice  $\mathbf{v}_k$  is covered by at least one BS.  $C(\mathbf{v}_k)$  is given by

$$C(\mathbf{v}_k) = \begin{cases} 1, & P_{BS_i}(\mathbf{v}_k) \geq \tau, \\ 0, & \text{otherwise,} \end{cases} \quad (6)$$

where  $\tau$  is the received power threshold.

Let  $\kappa$  denotes the COR, we have

$$\kappa = \frac{N_{\text{over}}}{N_t}, \quad (7)$$

where  $N_{\text{over}}$  denotes the number of lattices belonging to the coverage overlap.  $N_{\text{over}}$  is given by

$$N_{\text{over}} = \sum_{k=1}^{N_t} O(\mathbf{v}_k), \quad (8)$$

where  $O(\mathbf{v}_k)$  denotes whether the lattice  $\mathbf{v}_k$  is covered by more than one BS.  $O(\mathbf{v}_k)$  is given by

$$O(\mathbf{v}_k) = \begin{cases} 1, & \exists (P_{BS_i}(\mathbf{v}_k) \geq \tau) \& (P_{BS_{j \neq i}}(\mathbf{v}_k) \geq \tau), \\ 0, & \text{otherwise.} \end{cases} \quad (9)$$

In this paper, we aim at maximizing the coverage for 3D airspace while controlling overlap. This objective can be transformed into a problem of maximizing coverage subject to overlap constraints. In particular, the optimization problem can be formulated as

$$\mathbf{P1} : \max_{\{\Psi, \Phi, \Theta\}} \xi \quad (10)$$

$$\text{C1} : 0 < \Psi < 180^\circ, \quad (10a)$$

$$\text{C2} : 0 < \Phi < 180^\circ, \quad (10b)$$

$$\text{C3} : -90 \leq \Theta \leq 90^\circ, \quad (10c)$$

$$\text{C4} : 0 \leq \kappa \leq T, \quad (10d)$$

where  $T$  denotes the level of controlled overlap. In **P1**, C1-C3 limit the tuning range of the beam parameters, and C4 limits the coverage overlap ratio of the given 3D airspace. It is shown that problem **P1** is a non-convex mixed integer optimization problem.

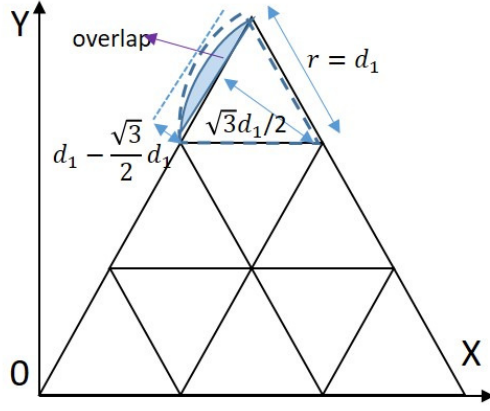


Fig. 2. Illustration of the TP coverage structure.

### III. COVERAGE MAXIMIZATION SCHEME BASED ON COTP MODEL

In this section, we prove the minimum coverage overlap property of the cooperation among three TBSs and design the CoTP coverage model. Based on this model, a coverage structure based on the Delaunay triangulation (DT) and the cooperative beam generation algorithm are proposed for G2A coverage extension.

#### A. CoTP Coverage Model

It is well-known that the square, triangle, and hexagon are regarded as potential coverage structures in the context of cellular network planning. To extend G2A coverage, three prisms can be constructed by extending these three planar structures vertically, including TP, square-prism (SP), and hexagonal-prism (HP). Then, we compare the airspace coverage of the three prism-shaped coverage structures.

**Proposition 1.** Let  $\zeta_1, \zeta_2, \zeta_3$  denote the inter-region overlap ratio of the TP, SP, and HP coverage structures, respectively, with guaranteed seamless coverage. The inequality  $\zeta_1 < \zeta_2 < \zeta_3$  holds.

*Proof.* When a TBS is equipped with directional antennas, its coverage takes on an approximately cone-shaped space. The coverage radius of the TBS is denoted as  $r$ , while  $d_1, d_2$ , and  $d_3$  denote the inter-site distance between TBSs for the TP, SP, and HP coverage structures, respectively. Considering the macro TBS, the height of the low-altitude space is denoted as  $H$ , where  $0 < H < r$ . The inter-region coverage overlap ratio is defined as the ratio of the TBS signal coverage volume exceeding the coverage structure's range to the total volume.

The vertical view of the TP structure is shown in Fig. 2. The area of the regular triangular region with side length  $d_1 = r$  is given by  $s_1 = \sqrt{3}d_1^2/4$ . The volume of the TP airspace is given by  $V_1 = s_1H$ . The blue arched region represents the inter-region overlap. As it rotates in 3D space, the arched region becomes a spherical segment. The volume of a spherical segment is given by  $V_{11} = \pi(d_1 - \sqrt{3}d_1/2)^2(r - (d_1 - \sqrt{3}d_1/2)/3)$ . Then,  $\zeta_1$  is given by

$$\zeta_1 = \frac{3V_{11}}{V_1} = \frac{(16\sqrt{3} - 27)\pi r}{6H} \approx 0.37r/H. \quad (11)$$

The vertical view of the SP structure is shown in Fig. 3. The area of the regular quadrangular with side length  $d_2 = \sqrt{2}r/2$  is given by  $s_2 = d_2^2$ . The volume of the SP airspace is given by  $V_2 = s_2H$ . The blue arched region contains the overlapped and non-overlapped parts. The volume of the spherical segment is given by  $V_{21} = \pi(\sqrt{2}d_2 - d_2)^2(r - (\sqrt{2}d_2 - d_2)/3)$ . In the blue region, the red triangular belongs to the non-overlapped part, forming a cone in the 3D airspace. The volume of the cone is given by  $V_{22} = \pi((\sqrt{2}d_2 - d_2)^2(\sqrt{2}d_2 - d_2)/3)$ . Then,  $\zeta_2$  is given by

$$\zeta_2 = \frac{4(V_{21} - V_{22})}{V_2} = \frac{4(\sqrt{2} - 1)\pi r}{3H} \approx 1.74r/H. \quad (12)$$

The vertical view of the HP structure is shown in Fig. 4. The area of the regular hexagonal with side length  $d_3 = r/2$ , is given by  $s_3 = 3\sqrt{3}d_3^2/2$ . The volume of the HP airspace is given by  $V_3 = s_3H$ . The blue arched region contains the overlapped and non-overlapped parts. The volume of the spherical segment is given by  $V_{31} = \pi(d_3)^2(r - d_3/3)$ . In the blue region, the red triangular and green rectangular belong to the non-overlapped parts, forming a cone and a cylinder in the 3D

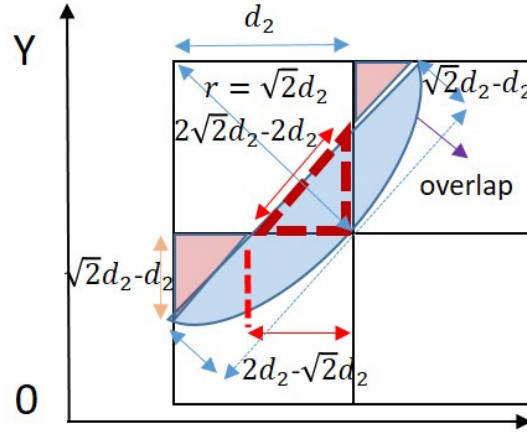


Fig. 3. Illustration of the SP coverage structure.

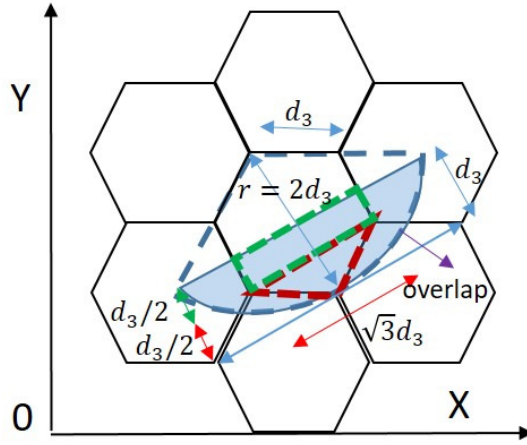


Fig. 4. Illustration of the HP coverage structure.

space, respectively. The volume of the red cone is given by  $V_{32} = \pi((\sqrt{3}d_3/2)^2(d_3/2))$ . The volume of the green cylinder is given by  $V_{33} = \pi((\sqrt{3}d_3/2)^2(d_3/6))$ . Then,  $\zeta_3$  is given by

$$\zeta_3 = \frac{6(V_{31} - V_{32} - V_{33})}{V_3} = \frac{7\pi r^3}{3\sqrt{3}r^2 H} \approx 4.23r/H. \quad (13)$$

Hence, we can obtain the inequality  $\zeta_1 < \zeta_2 < \zeta_3$ . □

The conclusion drawn from Proposition 1 is that the cooperation between three TBSs can obtain a minimum coverage overlap while ensuring seamless coverage. Therefore, we propose the CoTP model, which is based on cooperation among three TBSs. As shown in Fig. 5, all TBSs deployed on plane  $P$  are clustered into multiple TBS sets, and each set includes three TBSs, such as  $\{BS_1, BS_2, BS_3\}$ . The triangle-shaped region  $P_1$  is created by connecting each pair of BSs in  $\{BS_1, BS_2, BS_3\}$ . Correspondingly, the given region  $P \in \mathbb{R}^2$  is divided into multiple triangular-shaped regions. A TP-shaped airspace  $\Omega_1$  is formed by extending  $P_1$  along the vertical direction. Then, the airspace  $\Omega_1$  is divided into three subspaces, including the low-layer, the medium-layer, and the high-layer, denoted as  $\{L_1, L_2, L_3\}$  and served by the antennas of  $\{BS_1, BS_2, BS_3\}$  with different parameters  $\{\epsilon_1, \epsilon_2, \epsilon_3\}$ , respectively.

#### B. Coverage Structure Based on Delaunay Triangulation

Based on the CoTP model, we design the Delaunay triangulation (DT)-based cooperative coverage structure to enhance G2A coverage extension. The DT satisfies both the empty circumcircle (EC) criterion and the maximized minimum internal

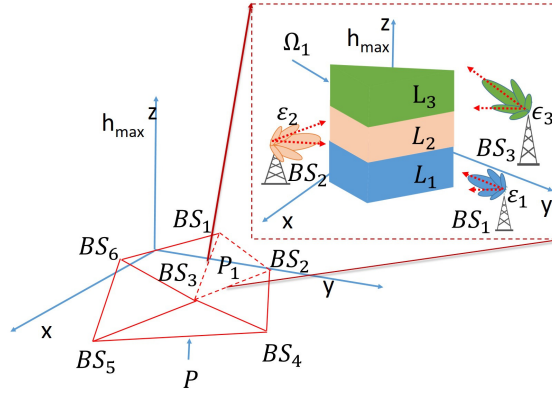


Fig. 5. Illustration of the CoTP model.

angle (MIAM) criterion [21], and its excellent coverage ability has been extensively verified [22]. Furthermore, the DT-based coverage structure provides an advantage in controlling intra-region overlap.

**Proposition 2.** *If the antenna radiation radius of three TBSs located at the vertices of a triangle are equal, and the seamless coverage of a triangle-shaped region is guaranteed, then the ratio of intra-region overlap decreases as the length of the longest edge of the triangle decreases.*

*Proof.* Let  $S_0$ , and  $L$  denote the area and the length of the longest edge of the triangle, respectively. For a given triangle-shaped region,  $S_0$  remains constant.

To ensure seamless coverage of the triangle-shaped region, the transmission power of the antenna is determined by the length of the longest edge  $L$ . Because the radiation radius of three TBSs located at the vertices of a triangle are the same, this radius can be denoted as  $R = 0.5L$ . Then, the total coverage area of all corresponding antennas can be calculated as

$$S = \sum_{i=1,2,3} \frac{n_i \pi R^2}{360}, \quad (14)$$

where  $n_1$ ,  $n_2$ , and  $n_3$  are the inner angles of the triangle. Due to  $n_1 + n_2 + n_3 = 180^\circ$ , we have  $S = 0.5\pi R^2$ . As  $L$  decreases,  $R$  and  $S$  also decrease.

Therefore, we can conclude that the coverage overlap ratio, which is given as  $\zeta = (S - S_0)/S_0$ , also decreases as the length of the longest edge of the triangle decreases.  $\square$

The DT can minimize the length of the longest edge of the triangle statistically [21]. Based on the conclusion of Proposition 2, the DT-based coverage structure can minimize the intra-region overlap statistically. With the DT-based coverage structure, all TBSs in a cellular network are clustered into multiple TBS sets, and each set contains three TBSs. The plane enclosed by three TBSs in each set can be vertically extended into a TP-shaped airspace.

### C. Space Layered Beam Cooperative Coverage Algorithm

In the paper [23], the authors proposed a randomized optimization method designed for clustered networks. Drawing inspiration from this, we have devised a Particle Swarm Optimization (PSO)-based algorithm specifically tailored for each clustered network. In the TP-shaped airspace, the PSO-based SLBC coverage algorithm for obtaining optimal beam parameters is proposed. The SLBC algorithm can tackle the challenge arising from the coexistence of continuous and discrete variables. As shown in Fig. 6, three beams of  $\{BS_1, BS_2, BS_3\}$  implement cooperative airspace coverage. For the existing antenna, the H-HPBW and V-HPBW are discrete while the tilt angle is continuous [24]. Especially, the beam pattern determines the H-HPBW and V-HPBW. In the SLBC, two groups of particle swarms work separately. The discrete one  $\Xi_1$  corresponds to the beam pattern while the continuous one  $\Xi_2$  corresponds to the tilt angle. Both groups search for solutions independently and share the same fitness function (10).

To explore the solution,  $N$  particles search in the  $M$ -dimensional solution space. During the  $l$ -th iteration, the tilt angle optimization task in swarm  $\Xi_1$  involves updating the velocity and position of each particle according to (15),

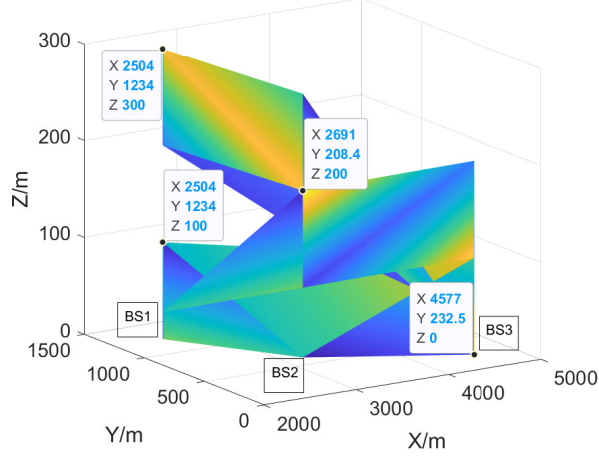


Fig. 6. The diagram of cooperative beam coverage.

$$\begin{cases} V_m(l+1) = wV_m(l) + c_1 F_1(S_L^*(l) - B_m(l)) \\ \quad + c_2 F_2(S_G^*(l) - B_m(l)), \\ B_m(l+1) = B_m(l) + V_m(l+1), m \in [1, M], \end{cases} \quad (15)$$

where  $w$  denotes the inertia weight,  $S_L^*(l)$  denotes the local best position, and  $S_G^*(l)$  denotes the global best position. Moreover,  $F_1$  and  $F_2$  are a pair of random coefficients.  $c_1$  and  $c_2$  denote the local and global learning coefficients, respectively. The learning coefficient controls the step size of particle position updates based on individual experience and group cooperation. The inertia weight reflects the tendency of particles to maintain their current velocity. Generally, the inertia weight  $w$  gradually decreases during iterations to encourage particles to converge throughout the search process, as given by  $w = w_{\max} - (l - 1) \times (w_{\max} - w_{\min}) / (N_{\text{iter}} - 1)$ , where  $N_{\text{iter}}$  denotes the total number of iterations,  $w_{\max}$  and  $w_{\min}$  denote the bounds of inertia weight.

In addition, each particle in swarm  $\Xi_2$  performing the beam pattern optimization task requires a discrete version of iteration to update their velocity and position, following equation (16),

$$\begin{cases} G_m(l+1) = gG_m(l) + d_1 F_1(S_L^*(l) - X_m(l)) \\ \quad + d_2 F_2(S_G^*(l) - X_m(l)), \\ X_m(l+1) = \lceil X_m(l) + G_m(l+1) \rceil, m \in [1, M], \end{cases} \quad (16)$$

where  $\lceil \cdot \rceil$  denotes the operation of rounding down. Different from the general PSO, the iteration is performed under the constraint of overlap ratio, as described in (10d). Each of two particle swarms has the parameter  $M = 3$ , corresponding to three TBSs. The SLBC algorithm is summarized in Algorithm 1.

#### D. Adaptive Beam Cooperative Coverage Algorithm

To track the challenge posed by the limited number of beam patterns, a novel algorithm is required to improve the coverage of arbitrary triangular-shaped airspace. Additionally, it is crucial to prevent power leakage into adjacent TP-shaped spaces. Thus, the ABC algorithm is designed to determine the optimal and continuous H-HPBW, V-HPBW, and tilt angle.

Considering that the ABC algorithm originates from the PSO, the particles search for the solution in  $M$ -dimensional solution space  $S = \{\Omega_1, \Omega_2, \Omega_3, V_1, V_2, V_3, \theta_1, \theta_2, \theta_3\}$ , where  $\Omega_1, \Omega_2, \Omega_3$  denote continuous H-HPBW,  $V_1, V_2, V_3$  denote continuous V-HPBW, and  $\theta_1, \theta_2, \theta_3$  denote the continuous tilt angle of three TBSs, respectively. In addition, the flow of the ABC algorithm is similar to that of the general PSO algorithm.

## IV. NUMERICAL RESULTS

In this section, we present simulations and field trials to evaluate the performance of the CoTP-based G2A coverage extension method.

---

**Algorithm 1** SLBC coverage algorithm

---

**Input:** Initialize the learning coefficients, the inertia weight of particle swarms.**Output:** The optimal GCR.

```
1: Initialization
2: Randomly initialize the positions, velocity of  $N$  particle swarms in  $\Xi_1$  and  $\Xi_2$ .
3: Calculate the global best fitness value of all particles according to (10).
4: Calculate the global best position of particles in  $\Xi_1$  and  $\Xi_2$ .
5: for  $i$  in range  $N_{iter}$  do
6:   for  $j$  in range  $N$  do
7:     Update the velocity and position of  $\Xi_1$  as (15).
8:     Update the velocity and position of  $\Xi_2$  as (16).
9:     Calculate the GCR and COR according to (10).
10:    if COR satisfies the constraint (10d) then
11:      Update local best fitness value of particle swarms.
12:      Update local best position of particle swarms.
13:    end if
14:  end for
15: Update the global best fitness value of particle swarms.
16: Update the global best position of all particle swarms.
17: end for
18: return The optimal GCR.
```

---

Table I  
THE PERFORMANCE OF THE CoTP-BASED COVERAGE EXTENSION METHOD.

TBS set	$\alpha_1$	$\alpha_2$	$\alpha_3$	$b$	$v_1$	$v_2$
$X_1X_2X_7$	5	171	5	0.61	0.51	0.84
$X_1X_2X_4$	140	15	25	0.67	0.85	0.95
$X_1X_4X_5$	25	121	34	0.66	0.80	0.98
$X_1X_5X_6$	34	35	111	2.22	0.88	0.95
$X_2X_3X_4$	27	54	99	0.97	0.9	0.95
$X_2X_3X_7$	23	82	75	1.36	0.91	0.94
$X_3X_4X_5$	70	74	36	1.56	0.87	0.94
$X_5X_6X_9$	65	75	40	4.62	0.87	0.92
$X_6X_8X_9$	61	66	53	2.5	0.9	0.93

### A. Simulation Results

In the simulations, the environment parameters are set as  $h_{max} = 300\text{m}$ ,  $\tau = -90\text{dBm}$ , and  $P_T = 46\text{dBm}$  [17]. The learning coefficients and inertia weights are set as  $c_1 = d_1 = 1.5$ ,  $c_2 = d_2 = 2.5$ ,  $w_{min} = 0.4$ , and  $w_{max} = 0.9$ .  $a_1, a_2$ , and  $a_3$  denote three inner angles of a given triangle. The coverage ratio obtained in a TP airspace is treated as the optimal GCR.  $v_1$  and  $v_2$  are used to denote the optimal GCR based on the SLBC algorithm and ABC algorithm, respectively. In order to evaluate the G2A coverage extension in large-scale networks, the average GCR is defined as  $\rho = \sum_{t=1}^D b_t s_t / \sum b_t$ , where  $b_t$  and  $s_t$  denote the area of each triangle-shaped region and the optimal GCR of each TP-shaped airspace.  $D$  represents the number of DT-based triangular regions.

We simulate the GCR of a synthetic network that follows the configuration of a real-world operator's network, as shown in Fig. 11a. The simulation area comprises 9 TBSs, covering a 15 square kilometer region. The results are depicted in Table I. When the COR is 0.01%, the average GCR with the SLBC algorithm can reach 86%, while the average GCR with the ABC algorithm is over 93%. The average GCR of the ABC algorithm is higher than that of the SLBC algorithm. The advantage of the ABC algorithm is derived from its continuous adjustment of the H-HPBW and V-HPBW parameters.

The simulation results using a random plane division method are presented in Table II. Comparing the results in Table I and Table II, it is observed that the average GCR of the DT-based coverage structure is 86%, whereas the coverage structure based on the random plane division achieves an average GCR of 78% with the SLBC algorithm. Therefore, it can be concluded that the DT-based coverage structure is better than the coverage structure based on the random plane division method. With the ABC algorithm, the conclusion still holds.

To illustrate the performance of the SLBC algorithm and ABC algorithm, a simulation is conducted in the triangle-shaped region enclosed by  $X_2, X_3, X_4$ , where three inner angles are  $a_1 = 99^\circ, a_2 = 54^\circ, a_3 = 27^\circ$ .

Fig. 7 depicts the performance of the SLBC algorithm. The simulation results demonstrate that the SLBC algorithm can rapidly converge, and the optimal GCR can reach 90% while the COR is 0.01%. Moreover, the optimal tilt angle, H-HPBW, V-HPBW for three TBSs located in the TP-shaped airspace are  $\{-52^\circ, 15^\circ, 25^\circ\}, \{-13^\circ, 110^\circ, 25^\circ\}, \{9^\circ, 110^\circ, 25^\circ\}$ , respectively. The tilt angles indicate the subspace in the TP-shaped airspace that each antenna is responsible for. The optimal parameters

Table II  
THE PERFORMANCE OF COVERAGE EXTENSION METHOD BASED ON RANDOM DIVISION.

TBS set	$\alpha_1$	$\alpha_2$	$\alpha_3$	$b$	$v_1$	$v_2$
$X_3X_5X_7$	172	4	4	0.43	0.55	0.88
$X_2X_5X_7$	141	20	19	2.14	0.81	0.94
$X_1X_2X_7$	5	171	5	0.61	0.51	0.84
$X_2X_4X_5$	33	100	47	1.31	0.90	0.94
$X_1X_2X_4$	140	15	25	0.67	0.85	0.95
$X_1X_4X_5$	25	121	34	0.66	0.80	0.98
$X_5X_8X_9$	19	35	126	3.47	0.80	0.86
$X_1X_5X_8$	101	55	24	4.89	0.79	0.87
$X_1X_6X_8$	11	159	10	0.99	0.75	0.89

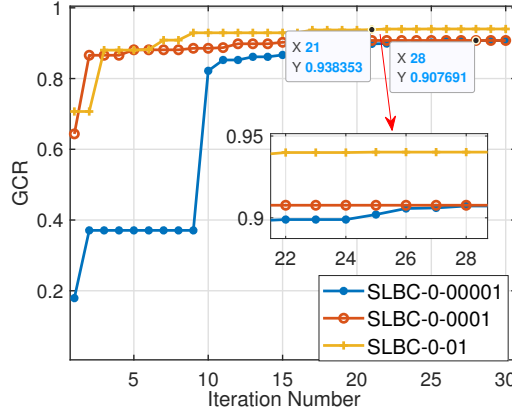


Fig. 7. The convergence of the SLBC algorithm. SLBC-0.00001, SLBC-0.0001, and SLBC-0.01 represent the cases where the COR values are 0.00001, 0.0001, and 0.01, respectively.

obtained in the simulation provide valuable guidance for G2A coverage extension. However, it is worth noting that the beam power may leak to adjacent TP-shaped airspace since the H-HPBW value of  $110^\circ$  exceeds  $a_2$  and  $a_3$ . The result means that the width of the beam is wider than the given region.

The simulation results in Fig. 8 demonstrate that the ABC algorithm can rapidly converge, and the optimal GCR can reach 95% while the COR is 0.01%. Moreover, the optimal tilt angle, H-HPBW, V-HPBW of three TBSs are  $\{-80^\circ, 77^\circ, 112^\circ\}$ ,  $\{-21^\circ, 35^\circ, 41^\circ\}$ ,  $\{14^\circ, 27^\circ, 129^\circ\}$ , respectively. Note that the H-HPBW values of all TBSs are smaller than the width of the given region. This ensures that the main lobe of the antenna beam falls within the triangular coverage region and avoids power leakage to adjacent TP airspace.

Furthermore, we assess the GCR of the ABC and SLBC by comparing them to the exhaustive search (ES) algorithm and the algorithm that utilizes the 5G beam without 3D cooperation (5G Beam W/O) [24].

The GCR under different received power thresholds is shown in Fig. 9. It is observed that as the threshold increases, the GCR decreases. Furthermore, the GCR of the ABC closely aligns with that of the ES algorithm, exceeding the GCR of the 5G beam-based algorithm without cooperation.

The GCR under varying maximum heights is shown in Fig. 10. It should be noted that an increase in the maximum height of the covered airspace results in a slight decline in the GCR. Nonetheless, the proposed algorithm can maintain robust 3D coverage performance even as height increases. This suggests that the proposed algorithms obtain robust adaptability to variations in coverage height.

### B. Field Trials

The field trials are conducted in a typical suburban region in Zigong, a city located in southwest China. The networks include 9 TBSs, covering a region of 15 square kilometers. The network topology is shown in Fig. 11a, with  $\{X_1, X_2, \dots, X_9\}$  representing the locations of the 9 TBSs. Multiple triangular-shaped regions have been designed using the DT-based coverage structure generating method.

The field trials are implemented by a UAV and two drive-test terminals (see Fig. 11b). The gathered samples from two drive-test terminals are labeled D1 and D2, respectively. On the drive-test terminals, the Huawei AAU5613 5G antennas are employed. The beam patterns are configured according to the 5G antenna mode [24]. Due to operational limitations, we restrict

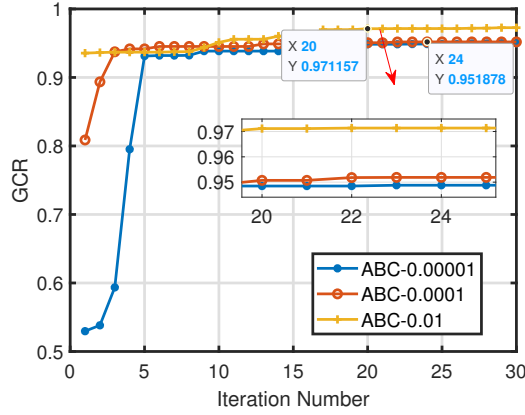


Fig. 8. The convergence of the ABC algorithm. ABC-0.00001, ABC-0.0001, and ABC-0.01 represent the cases where the COR values are 0.00001, 0.0001, and 0.01, respectively.

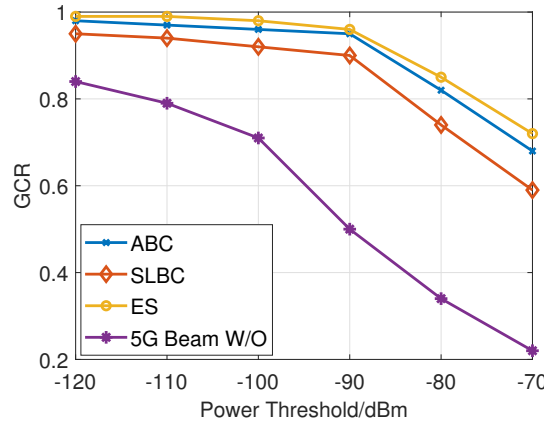


Fig. 9. The coverage for airspace with varying received power thresholds.

the range of tilt angle to  $[-15^\circ, 15^\circ]$ . The sample tasks are implemented at different altitudes (Fig. 11c, see Fig. 11d). The detailed parameters of the field trial are shown in Table III.

The coverage performance comparison between the down-tilted antennas and the configurations based on the SLBC is shown in Table IV. We can observe that the network with down-tilted antennas achieves an average GCR of around 46.05%, while the network with the antenna configurations based on the SLBC algorithm obtains an average GCR of around 84.56%. It is concluded that the GCR of the CoTP-based method improves by 83% compared to a cellular network that uses down-tilted antennas.

Fig. 12 displays the GCR of sub-layer airspace with different heights, presenting both the simulation results and field trials derived from the CoTP-based method and down-tilted antennas. It is observed that the CoTP-based method enhances the coverage of each sub-layer of the total airspace, with a particular emphasis on ensuring coverage for near-ground sub-layers, including (0-50)m and (50-100)m.

## V. CONCLUSION

In this paper, we proposed a CoTP-based G2A coverage extension method for beyond 5G networks. The proposed method aims to maximize the coverage ratio of 3D airspace while controlling overlap, achieved by designing the TBSs cooperative set and antenna parameters in existing cellular networks. First, we designed the CoTP model and the coverage structure based on Delaunay triangulation. Then, the SLBC algorithm has been designed to obtain sub-optimal antenna parameters. To further improve the coverage ratio in 3D airspace, the ABC algorithm has been designed, which can also address the power leakage problem. Finally, the simulation results and field trials revealed the effectiveness of the CoTP-based G2A coverage extension method.

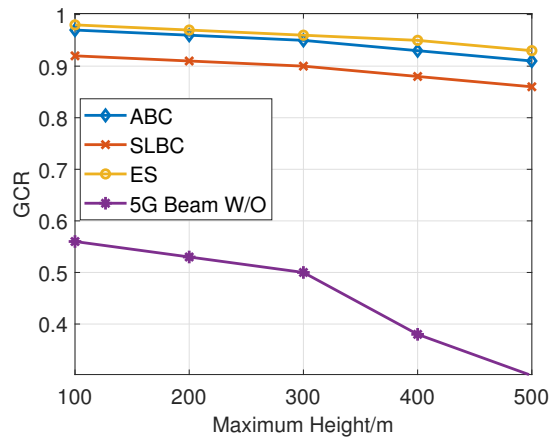


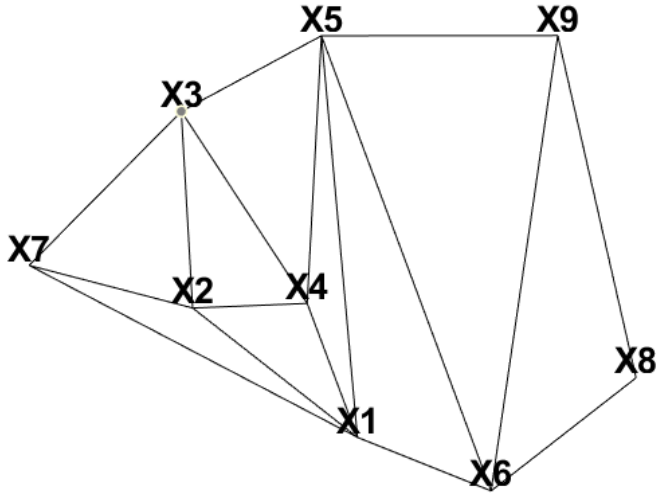
Fig. 10. The coverage for airspace with varying maximum heights.

Table III  
PARAMETERS OF THE FIELD TRIAL.

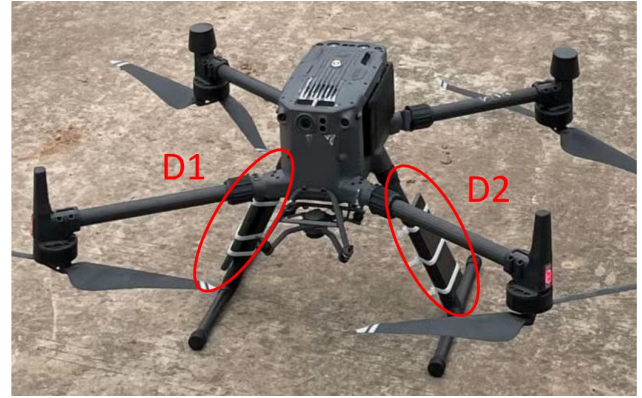
Parameters	Configuration
Propagation environment	Suburban
Frequency	2.6GHz
Antenna	64T×64R
Number of aerial samples	5000×6
Speed of UAV	15m/s
Flight altitude	{75,100,150,200,250,300}m
Sample rate	1Hz

## REFERENCES

- [1] Y. Zeng, J. Lyu, and R. Zhang, "Cellular-connected UAV: potential, challenges, and promising technologies," *IEEE Wireless Communications*, vol. 26, no. 1, pp. 120–127, 2019.
- [2] Y. Li, T. Jiang, M. Sheng, and Y. Zhu, "Qos-aware admission control and resource allocation in underlay device-to-device spectrum-sharing networks," *IEEE Journal on Selected Areas in Communications*, vol. 34, no. 11, pp. 2874–2886, 2016.
- [3] R. Amer, W. Saad, and N. Marchetti, "Mobility in the sky: Performance and mobility analysis for cellular-connected UAVs," *IEEE Transactions on Communications*, vol. 68, no. 5, pp. 3229–3246, 2020.
- [4] N. Cherif and W. Jaafar, "3D aerial highway: The key enabler of the retail industry transformation," *IEEE Communications Magazine*, vol. 59, no. 9, pp. 65–71, 2021.
- [5] S. J. Maeng and M. M. U. Chowdhury, "Base station antenna uptilt optimization for cellular-connected drone corridors," *IEEE Transactions on Aerospace and Electronic Systems*, pp. 1–9, 2023.
- [6] Y. Liu, W. Huangfu, H. Zhang, and K. Long, "An efficient stochastic gradient descent algorithm to maximize the coverage of cellular networks," *IEEE Transactions on Wireless Communications*, vol. 18, no. 7, pp. 3424–3436, 2019.
- [7] E. Balevi and J. G. Andrews, "Online antenna tuning in heterogeneous cellular networks with deep reinforcement learning," *IEEE Transactions on Cognitive Communications and Networking*, vol. 5, no. 4, pp. 1113–1124, 2019.
- [8] M. Sheng, C. Yang, Y. Zhang, and J. Li, "Zone-Based Load Balancing in LTE Self-Optimizing Networks: A Game-Theoretic Approach," *IEEE Transactions on Vehicular Technology*, vol. 63, no. 6, pp. 2916–2925, 2014.
- [9] M. M. Azari and F. Rosas, "Ultra reliable UAV communication using altitude and cooperation diversity," *IEEE Transactions on Communications*, vol. 66, no. 1, pp. 330–344, 2018.
- [10] N. Cherif and Alzenad, "Downlink coverage and rate analysis of an aerial user in vertical heterogeneous networks (VHetNets)," *IEEE Transactions on Wireless Communications*, vol. 20, no. 3, pp. 1501–1516, 2021.
- [11] J. Li, Z. Haas, and M. Sheng, "Capacity evaluation of multi-channel multi-hop ad hoc networks," in *2002 IEEE International Conference on Personal Wireless Communications*, 2002, pp. 211–214.
- [12] M. M. Azari, F. Rosas, A. Chiumento, and S. Pollin, "Coexistence of terrestrial and aerial users in cellular networks," in *IEEE Globecom Workshops (GC Wkshps)*, 2017, pp. 1–6.
- [13] M. Mozaffari, X. Lin, and S. Hayes, "Toward 6G with connected sky: UAVs and beyond," *IEEE Communications Magazine*, vol. 59, no. 12, pp. 74–80, 2021.
- [14] J. Lyu and R. Zhang, "Network-connected UAV: 3-D system modeling and coverage performance analysis," *IEEE Internet of Things Journal*, vol. 6, no. 4, pp. 7048–7060, 2019.
- [15] Y. Li and M. Xia, "Ground-to-air communications beyond 5G: A coordinated multi-point transmission based on poisson-delaunay triangulation," *IEEE Transactions on Wireless Communications*, pp. 1–1, 2022.
- [16] C. Zhou, J. Liu, M. Sheng, Y. Zheng, and J. Li, "Exploiting Fingerprint Correlation for Fingerprint-Based Indoor Localization: A Deep Learning Based Approach," *IEEE Transactions on Vehicular Technology*, vol. 70, no. 6, pp. 5762–5774, 2021.
- [17] TR36.777, "Study on enhanced LTE support for aerial vehicles(Release 15)," *3rd Generation Partnership Project(3GPP)*, 2017.
- [18] J. Liu, M. Sheng, R. Lyu, Y. Shi, and J. Li, "Access points in the air: Modeling and optimization of fixed-wing UAV network," *IEEE Journal on Selected Areas in Communications*, vol. 38, no. 12, pp. 2824–2835, 2020.



(a) The TBSs deployment topology.



(b) The drive-test equipment.



(c) UAV control terminal.



(d) UAV performing tasks.

Fig. 11. The field trial.

- [19] H. Ozpinar and Aksimsek, "A novel compact, broadband, high gain millimeter-wave antenna for 5G beam steering applications," *IEEE Transactions on Vehicular Technology*, vol. 69, no. 3, pp. 2389–2397, 2020.
- [20] D. Fagen and P. A. Vicharelli, "Automated wireless coverage optimization with controlled overlap," *IEEE Transactions on Vehicular Technology*, vol. 57, no. 4, pp. 2395–2403, 2008.
- [21] A. Okabe, B. Boots, and K. Sugihara, "Spatial tessellations concepts and applications of voronoi diagrams," *New York: Wiley*, 1992.
- [22] M. Abedi and R. Wichman, "Cellular network planning under variable QoS requirements using voronoi algorithm," in *IEEE Wireless Communications and Networking Conference (WCNC)*, 2020, pp. 1–6.
- [23] D. Zhou, M. Sheng, B. Li, J. Li, and Z. Han, "Distributionally robust planning for data delivery in distributed satellite cluster network," *IEEE Transactions on Wireless Communications*, vol. 18, no. 7, pp. 3642–3657, 2019.
- [24] F. Jesus and M. Sousa, "Evaluating 5G coverage in 3D scenarios under configurable antenna beam patterns," in *24th International Symposium on Wireless Personal Multimedia Communications (WPMC)*, 2021, pp. 1–6.

Table IV

THE REAL-WORLD MEASUREMENT COVERAGE PERFORMANCE COMPARISON BETWEEN THE DOWN-TILTED ANTENNAS AND THE SLBC-BASED METHOD.  
 \*-ORI DENOTES THE DOWN-TILTED ANTENNAS. \*-OPTI DENOTES THE CONFIGURATIONS BASED ON THE SLBC-BASED METHOD. D1 AND D2 REPRESENT TWO DIFFERENT DRIVE-TEST TERMINALS.

Parameters	D1-ori	D2-ori	D1-opti	D2-opti
X <sub>2</sub> -Beam (Pattern)	2	2	7	7
X <sub>2</sub> -Tilt (°)	-3	-3	3	3
X <sub>3</sub> -Beam (Pattern)	3	3	8	8
X <sub>3</sub> -Tilt (°)	-3	-3	7	7
X <sub>4</sub> -Beam (Pattern)	4	4	9	9
X <sub>4</sub> -Tilt (°)	-1	-1	11.5	11.5
GCR	45.87%	46.23%	84.23%	84.89%

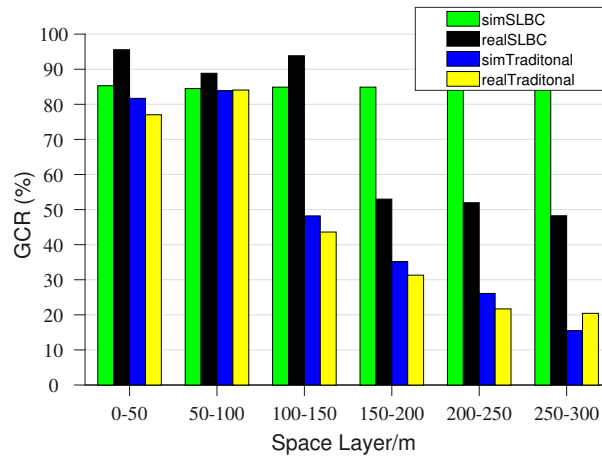


Fig. 12. The coverage of varying subspace. The green bars represent the simulated GCR with the CoTP-based method, while the black bars represent the corresponding measurements in the real world. The blue bars represent the simulated GCR with down-tilted antennas, while the yellow bars represent the measurements with down-tilted antennas.